Optimization of the pulse-compression technique applied to the infrared thermography nondestructive evaluation.

Giuseppe Silipigni[1], Pietro Burrascano[1], David. A. Hutchins[2], Stefano Laureti[1,2], Roberto Petrucci[3], Luca Senni[1], Luigi Torre[3], and Marco Ricci[4*],

[1]Dipartimento di Ingegneria, Polo Scientifico Didattico di Terni, Università di Perugia,
Strada di Pentima 4, 05100 Terni, Italy
giuseppe.silipigni@studenti.unipg.it, {pietro.burrascano,luca.senni}@unipg.it

[2]School of Engineering, University of Warwick
Library Road, Coventry CV4 7AL, United Kingdom
{D.A.hutchins, S.Laureti}@warwick.ac.uk

[3]Dipartimento di Ingegneria Civile ed Ambientale, Polo Scientifico Didattico di Terni, Università di Perugia,
Strada di Pentima 4, 05100 Terni, Italy
{roberto.petrucci,luigi.torre}@unipg.it

[3]Dipartimento di Ingegneria Informatica, Modellistica, Elettronica e Sistemistica, Università della Calabria,
Via Pietro Bucci, 87036 Arcavacata, Rende CS
e-mail: m.ricci@dimes.unical.it

***Abstract*—** Pulse-compression infrared thermography is an emerging nondestructive testing and evaluation technique. An analysis of the main issues hampering the full exploitation of this technique is presented from both theoretical and experimental point of view and various strategies are introduced to overcome these problems and optimize the defect detection performance. A comparison between conventional pulse-compression thermography procedures and the proposed one is reported, using an LED modulated with a Barker sequence as coded excitation, and a carbon fibre composite benchmark sample containing artificial defects at different depths. The experimental results show that the suggested signal processing procedure assures a higher SNR and hence an improved defect detection capability. In addition, a time-analysis of such signals allows the correlation between the depth of defects and heat diffusion time to be more clearly identified.

Keywords—Nondestructive evaluation, Thermography, Coded Excitation, Pulse-compression, Barker Codes

I. INTRODUCTION

Active Thermography (AT) is a Non Destructive Testing (NDT) technique with application in various fields of research and analysis, ranging from diagnostic, material characterization to on-line and in-service inspection [1–6]. In particular, AT is applied extensively to the inspection of composite structures, and various measurement strategies have been developed to improve the technique [7–11]. Two main approaches have been pursued: time-domain analysis, with Pulsed Thermography (PT) as the most common method [12–15], and frequency-domain signals, with the single-frequency Lock-In Thermography (LIT) technique being the most popular [16–19]. The former approach provides more information than the latter. This is because a continuous frequency bandwidth is excited. On the other hand, by concentrating the signal energy within a limited set of excitation frequencies, use of a Lock-In produces improved levels of Signal-to-Noise Ratio (SNR) at the cost of less information. In recent years, many techniques have been developed in order to combine the advantages of both the above mentioned approaches, such as Pulsed-Phase Thermography (PPT) [4] and Multi-Frequency Lock-in Thermography (MF-LIT) [20].

Pulse-Compression Thermography (PuCT) is a recent technique developed by Mandelis *et al.* [21,22] and Mulaveesala *et al*. [23–25] in which the heating stimulus is in the form of a coded signal that has a unique characteristic: the bandwidth and the duration of the signal can be made mutually independent by proper code

design [26]. As a consequence, the frequency content of the signal can be tailored to the type of materials/defects under investigation, while the duration of the signal can be determined by considering the required SNR value. Moreover, with the use of coded excitation, both time and frequency domain processing can be implemented; the former can be retrieved after the application of the PuC step that outputs an estimate of the impulse response, while the latter can be directly performed on the acquired data. As a matter of fact, PuCT tries to retrieve the time and spatial resolution of PT with the SNR of LIT. In recent years, various PuC schemes have been proposed, which mainly differ in the type of coded waveforms used (binary sequences or frequency modulated "chirp" signal) or the type of heating source [21,27–30]. Note that coded excitation can also be used without PuC. For example, the performance of frequency modulated thermography has been compared with those of PT and LIT [31]. Nonetheless, some issues remain in PuCT since most of the implementations focus on the SNR gain and do not analyze the quality of the reconstruction of the impulse responses.

Our aim is thus to propose a measurement protocol that optimizes both the SNR gain and the quality of the impulse response reconstruction. To accomplish this aim, we firstly analyze the theoretical and practical limitations facing the full exploitation of PuCT in thermography. We then introduce measurement and processing strategies that reduce the effect of these limitations. A comparison between the current state-of-the-art and the proposed approach is made by using a benchmark sample made of carbon-fibre-reinforced-composite with various artificial defects at different depths, using a 200W LED system as heating source. The experimental validation uses a Barker Code excitation [32,33], although it should be noted that the analysis can be easily extended to other types of excitation, such as frequency modulated chirps.

The paper is organized as follows: Section II introduces the theoretical background of the thermography NDT and of the Pulse-Compression technique; Section III highlights the pros and cons of the PuC Thermography and introduces some measurement and processing procedures aimed at optimizing the achievable SNR, and Section IV introduces the hardware and software used experimentally and illustrates the results of the inspection focusing on the use of Barker codes. Conclusions are then presented in Section V.

II. THEORETICAL BACKGROUND

Heat transmission is a very complex phenomenon for which an easy mathematical description is possible only for ideal cases or when various approximations are made, depending also on the type of thermal source used and the related physical principle of heating [34]. Here we consider an *external* excitation through LED lamps that delivers energy to the sample's surface. In this case, heat propagation is usually approximated as a 1-D phenomenon with the thermal front propagating by diffusion from the sample surface to the inside of the sample and assuming a negligible contribution of lateral diffusion [35]. The presence of a subsurface defect such as a delamination, a void, etc., changes the heat diffusion rate locally and then causes local variations of the surface temperature. Hence, by analyzing the radiation emitted by the inspection surface, the presence of a defect can be inferred. Moreover, since the heat diffusion from the sample surface to its inner part is not instantaneous, defects located at different depths produce observable changes in the emitted radiation at different times, so that information about the defect depth can be in principle extracted by a time-analysis of the emitted radiation.

II.A Heat Theory and Pulse Thermography

To gain insight on this, it is useful considering a simplified 1D model and considering some special solutions of the corresponding heat equation [34], which can be described by

$$\frac{\partial^2 \Theta(z,t)}{\partial z^2} - \frac{c\rho}{k}\frac{\partial \Theta(z,t)}{\partial \mathrm{t}} = -\frac{q(z,t)}{k}. \tag{1}$$

Here, z is the direction perpendicular to the inspection surface, $\Theta(z,t)$ $[K]$ and $q(z,t)$ $[\frac{W}{m^3}]$ are the temperature of the sample and the heat source amplitude at position z and time t, c $[\frac{J}{kg\cdot K}]$ is the specific heat, ρ $[\frac{kg}{m^3}]$ is the density, and k $[\frac{W}{m\cdot K}]$ is the thermal conductivity. In the case of a sinusoidal *external* heat source with frequency f and acting only on the inspection surface (i.e. $q(z)=0$ for $z\neq 0$) of a semi-infinite body, Eq. 2 can be rearranged in the frequency domain in the form of a Helmholtz equation for $z>0$ as:

$$\frac{\partial^2\Theta(z,f)}{\partial z^2}-\sigma^2\Theta(z,f)=0 \tag{2}$$

where i is the imaginary unit, $\sigma=\sqrt{\frac{i2\pi f}{\alpha}}=(1+i)\sqrt{\frac{\pi f}{\alpha}}=\frac{(1+i)}{\mu}\,[\frac{rad}{m}]$ is the complex wavenumber, $\alpha=\frac{k}{c\rho}\,[\frac{m^2}{s}]$ is the thermal diffusivity and $\mu=\sqrt{\frac{\alpha}{\pi f}}\,[m]$ is thermal diffusion length. Using a boundary condition that the heat flux is continuous at the sample surface, the solution of Eq.2 is an evanescent wave of the form [36]:

$$\Theta(z,t)=\Theta_0 e^{-\frac{z}{\mu}}\cos(\frac{z}{\mu}-2\pi f t+\frac{\pi}{4}) \tag{3}$$

Eq. 3 implies that the mean energy transport is zero [36]: the heat flux decreases exponentially with depth on a characteristic scale μ, and as a rule of thumb, it is assumed that the excitation frequency $f_{opt}(d)$ that has the highest sensitivity with respect to defects at depth d from the inspection surface is approximately $f_{opt}(d)=\frac{\alpha}{\pi d^2}$, for which $\mu=d$. Eq.3 also indicates that in the most general case of an arbitrary heating source, the thermal front suffers from dispersion since different frequencies exhibit different diffusion phase, $v_p(f)$, and group, $v_g(f)$, velocities:

$$v_p(f)=2\pi f\mu=2\sqrt{\pi f\alpha};\; v_g(f)=\frac{d\omega(\xi)}{d\xi}=4\sqrt{\pi f\alpha}=2v_p(f); \tag{4}$$

where ξ is the real part of the complex wavenumber.

Since pulsed thermography is the most common thermographic NDT technique, it is worth considering what Eqs. 1-4 imply when the heat source is a short excitation modeled with a Dirac's Delta function $\delta(t)$, *i.e.* modeled as a finite amount of heat that is instantaneously transferred to the sample. Assuming a semi-infinite body and an external heat source, the solution of Eq.2 in this case is described by the expression [34]:

$$\Theta(z,t)=\Theta(z,0)+\frac{Q}{c\rho\sqrt{\pi\alpha t}}e^{-\frac{z^2}{4\alpha t}} \tag{5}$$

The excitation heat pulse does not travel through the sample with a constant velocity and unaltered shape because of dispersion, so that the original short pulse spreads out in time. As a consequence, the impulse response $h(j_x,j_y,z=0,t)$ of the generic (j_x,j_y) pixel at the surface is not simply a delayed and attenuated replica of the original excitation pulse, but is a decay function in which defect signatures appear as "smooth" and "slow" variations of the decays themselves. Dispersion hampers also the identification of the depth of defects, since it is not possible to easily assign a Time-of-Flight value to dispersive phenomena. To overcome this problem, usually an average diffusion velocity is considered and the defect location can be assessed by identifying the time delay at which the defect signal is maximum. The following argument is commonly found in the literature: if $f_{opt(d)}=\frac{\alpha}{\pi d^2}$ is the optimal frequency for the detection of a defect at depth d, for which $\mu=d$, and if $v_p(f_{opt})=2\frac{\alpha}{d}$ is the phase velocity at that frequency, then the maximum defect signal is expected approximately at a time [37]

$$t_{max}(d)\sim\frac{d}{v(d)}=\frac{d^2}{2\alpha} \tag{6}$$

Hence, from the experimental measurement of t_{max} the depths of defects can be estimated. Note that $t_{max}(d)$ coincides with the instant at which Eq. (5) reaches its maximum when $z = d$. Starting from these considerations, many advanced processing algorithms such as the Thermographic Signal Reconstruction (TSR) have been developed. These aim to further improve defect detection by extracting specific parameters for each pixel from an analysis of the whole time trend [12,15,38]. From the above, it is clear that an optimum measurement of the impulse-response is important not only for effective defect detection but also for defect classification purposes. For example, if the excitation pulse is too long, the signal of a single pixel cannot be considered as an impulse response, but instead it should be regarded as the signal coming from the convolution of the impulse response with the excitation waveform. This makes interpretation of the data more difficult, even if it increases the SNR for some defects [39]. With this background, it is now possible to thoroughly analyze how the Pulse Compression technique applies to AT.

II.B. Pulse-Compression basic theory

Pulse Compression is a well-known measurement technique used to experimentally estimate the impulse response of a Linear Time-Invariant (LTI) system in a noisy environment or in presence of very low SNR values. The basic principle at the heart of the technique can be expressed as follows: given a coded excitation $s(t)$ and an another signal $\Psi(t)$, the so-called matched-filter, such that their convolution (denoted by $*$) approximates the Dirac's Delta function $\delta(t)$, $s(t) * \Psi(t) = \tilde{\delta}(t) \sim \delta(t)$, the impulse response $h(t)$ can be estimated by exciting the LTI system with the signal $s(t)$ and then by convolving the system output $y(t)$ with $\Psi(t)$, see Fig.1. To demonstrate this, consider an output signal $y(t)$ resulting from a convolution between the input signal $s(t)$ and the impulse response $h(t)$ on which is superimposed an Arbitrary-White-Gaussian-Noise (AWGN) e(t) : $y(t) = h(t) * s(t) + e(t)$. By convolving $y(t)$ with the matched filter $\Psi(t)$ an estimate of the impulse response $h(t)$ is attained:

$$h_{es}(t) = y(t) * \Psi(t) = h(t) * \underbrace{s(t) * \Psi(t)}_{\sim \delta(t)} + e(t) * \Psi(t) \sim h(t) * \delta(t) + \tilde{e}(t) = h(t) + \tilde{e}(t) \quad (7)$$

Here it is assumed that $\Psi(t)$ and $e(t)$ are uncorrelated so that $\tilde{e}(t)$ is also AWGN but with a lower energy than $e(t)$. A thorough analysis of PuC lies beyond the scope of this work, for a detailed discussion of PuC see for instance [26]. Here it is enough to highlight that the main advantages of PuC over pulsed excitation is that at end of the procedure a close estimate of the impulse response is achieved, while delivering power to the system over an extended time period. In this way, it is possible to provide more energy, and hence to increase the SNR. The main drawback of PuC is the mathematical noise introduced by the approximation $\tilde{\delta}(t)$, which modifies the impulse response $h(j_x, j_y, t)$ of the (j_x, j_y) pixel even in the case of no noise, i.e. $\lim_{e(t) \to 0} h_{es}(t) = h(t) * \tilde{\delta}(t)$. The sidelobes of $\tilde{\delta}(t)$ can deteriorate the reconstruction of the impulse response. An extensive literature can be found on how to design the optimal coded waveform, on how to optimize $\tilde{\delta}(t)$, and on how to achieve the highest SNR, etc.[26,40–43]. For instance, it has been found that in terms of SNR the best choice for the matched filter is simply $\Psi(t) = s(-t)$, while in order to optimize the quality of the reconstruction the matched filter should be replaced by the Wiener filter with a proper regularization. The following Section focuses on the application of the PuC approach to AT highlighting the specific disadvantages both from a theoretical and an experimental point of view, and analyzes some strategies to overcome or to mitigate them

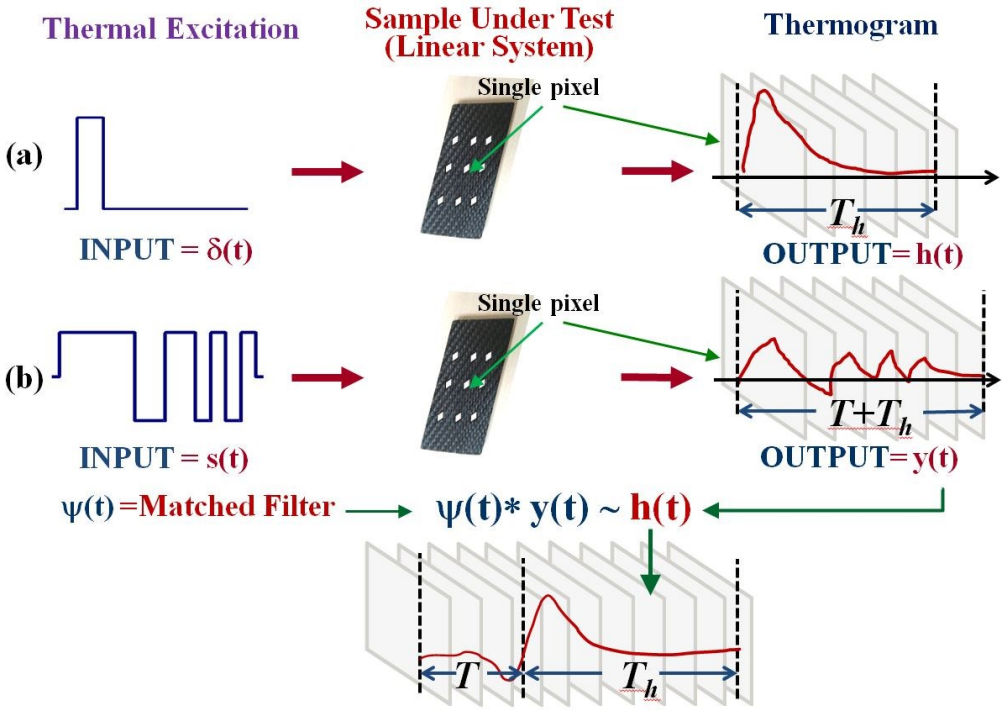

Fig. 1 Comparison between (a) Pulsed Thermography (PT) and (b) Pulse-Compression Thermography (PuCT). In PT the excitation is considered instantaneous and the sample impulse thermal response is measured for a time T_h, which is the expected duration of the impulse response of interest, i.e. the time necessary for the diffusion of the heat. In PuCT, the sample is excited with a coded excitation of duration T while thermograms are collected for a time ($T+T_h$). After the application of the PuC algorithm, an estimated impulse thermal response of duration T_h is retrieved.

III. Issues Affecting the Use of Pulse Compression in Active Thermography

For the use of the PuC in active thermography, there are two main practical issues that affect the full exploitation of the technique:

(A) The difficulty in realizing a bipolar heat source, as all heat sources used in thermography are unipolar, which will not normally generate PuC waveforms correctly;

(B) The need to concentrate the excitation energy at very low frequencies for ensuring sensitivity to hidden defects. This generally implies longer excitation times.

As a consequence of (A), the *true* excitation signal $s_{TR}(t) = s(t) + s_{SQ}(t)$ is a superposition of a coded excitation $s(t)$ and a square pulse $s_{SQ}(t) = C\{\vartheta(t) - \vartheta(t-T)\}$, where $\vartheta(t)$ is the Heaviside step function and T is the duration of the excitation. The *true* output signal will be $y_{TR}(t) = h(t) * s(t) + h(t) * s_{SQ}(t) + e(t) = y(t) + y_{SQ}(t)$, see Fig. 2. Therefore, before completing the PuC operation through the application of the matched filter, the contribution $y_{SQ}(t)$ of the square pulse to the acquired thermograms must be removed. To tackle this issue, in Subsection III-A, we analyze two different fitting procedures which are designed to remove the unwanted $y_{bias}(t)$ term. Moreover, the presence of the square pulse bias also determines the choice of the PuC measurement procedure. In [26] the main types of coded waveforms were analyzed in the light of the measurement scheme adopted, i.e. single-shot or continuous excitation. In AT, only the single shot procedure is possible in practice since the DC bias needs a finite time to reach a stable response. Thus, the correct PuCT procedure consists of:

(1) Exciting the sample with a coded excitation of duration T, (2) collecting thermograms for a time (T+T_h) where T_h is the expected duration of the impulse response of interest (i.e. the duration of the equivalent PT analysis), and (3) performing pixel-by-pixel the convolution with the matched filter to retrieve an estimation of the pixels impulse response of duration T_h, see Fig. 1.

In most of the cases reported to date, the thermograms were collected only when the coded excitation was switched on and then the PuC was performed by only analyzing the first T seconds. From a mathematical point of view such a strategy is correct only in the case of a periodic excitation, and when the steady-state is reached. It is worth stressing that, by truncating the acquisition of the output signal at T seconds, a further mathematical error is introduced in the reconstructed impulse response $h_{es}(t)$ in single-shot PuC besides the one entailed by $\tilde{\delta}(t)$. This error becomes negligible when T_h is significantly shorter than T, but this is not typically the case in PuCT. While such noise may not severely affect the defect detection task, it significantly hampers the defect classification process through time analysis of the impulse responses. To gain insight on this technical aspect that has nevertheless a strong impact on the PuCT performance, in Section IV a comparison between the "full" PuC procedure and the "truncated" one is reported.

Regarding point (B), due to the low thermal diffusivity of most composite and thermoplastic materials (α~10^{-6}-10^{-7} $[m^2/s]$), even defects at a depth of 1mm needs inspection frequencies in the range from tens to hundreds of millihertz. This affects the design of the optimal code for PuC and practically limits the SNR achievable by the use of PuC. Except for the complementary Golay code excitation, in general the amplitude of the $\tilde{\delta}'s$ sidelobes is inversely proportional to the Time-Bandwidth product TB of the waveform, which for binary codes coincides with the number of bits L. If we limit the bandwidth to fractions of Hertz, the code must last a few minutes to guarantee high TB products (TB>100), and this is not really suitable for on-line and/or in-situ inspections. As the SNR gain provided by PuC is proportional to the parameter TB, a trade-off between SNR, sidelobe levels and measurement time must be found. For low values of TB, an optimal choice is represented by the use of Barker Codes [32,33,41,42], which are the binary codes exhibiting the lowest sidelobes when

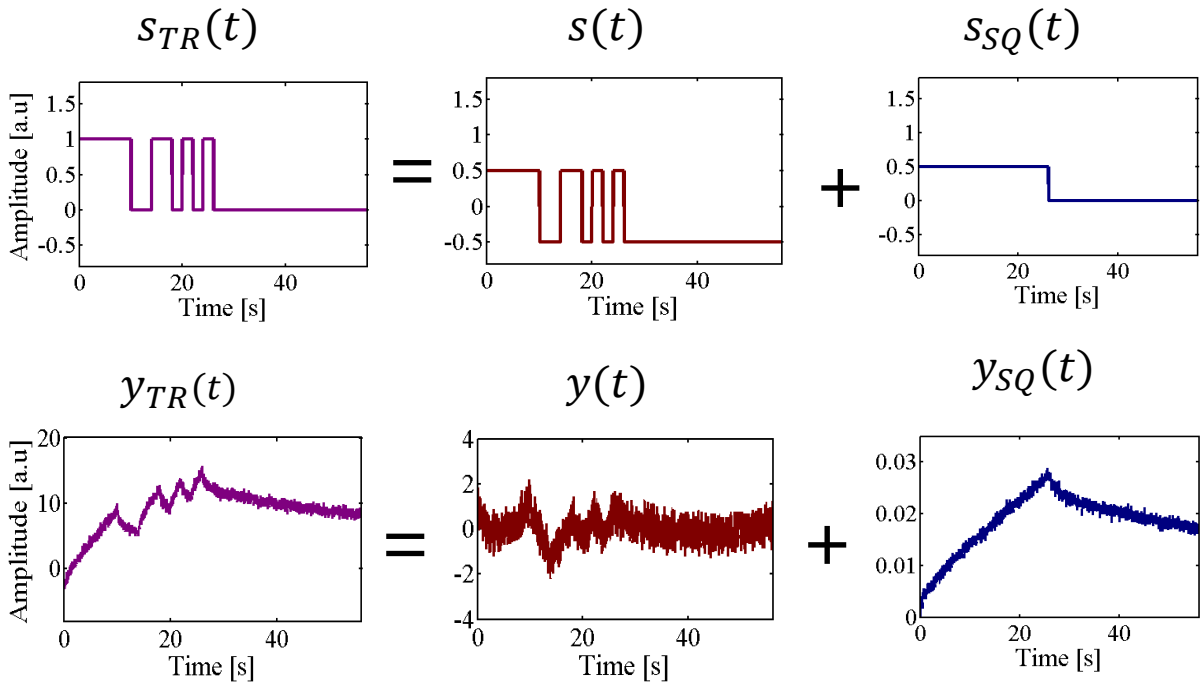

Fig.2: Typical "true" input $s_{TR}(t)$and output $y_{TR}(t)$ signals of a PuCT experiment: the input signal (top) is a superposition of the coded excitation $s(t)$ and of a square pulse $s_{SQ}(t)$. The output signal (bottom) is a superposition of a coded response $y(t)$ and of a step heating response $y_{SQ}(t)$.

used in a single-shot scheme. In addition, Barker codes do not require two or more measurements (as needed by complementary Golay codes for example), making them more suitable for Thermography over long measurement times. The main drawback of Barker codes is the fact that they exist only up to length $L=13$, which limits both the maximum theoretical SNR gain and the sidelobe suppression to ~22db. In Subsection III.B we illustrate how to modify the standard PuC to further reduce sidelobe amplitudes.

III.A Square pulse response removal

As stated above, practical PuCT applications require the removal of the underlying square pulse excitation contribution. To do this, a fitting procedure must be applied pixel-by-pixel to take the potential variations of each pixel's emissivity into account. Most authors report the use of a simple linear fit to remove the square pulse response [27,31]; however, this is too simplistic, leading to errors, and this in turn introduces further noise into the estimated impulse responses. Also, it is necessary to collect thermograms for a time T_h after the end of the coded excitation in order to estimate the first T_h seconds of the impulse responses. This means that the fitting function must be defined for $t>T$. Hence, even the decay curve must be separated into two contributions, one from the coded excitation $s(t)$, the other from the square pulse $s_{SQ}(t)$.

In order to perform this separation optimally, we tested the two excitation strategies depicted in Fig.3 by applying the two different fitting procedures described mathematically by the following expressions:

$$\text{Excitation Signal 1} - \text{"Single Barker"} \qquad \text{Excitation Signal 2} - \text{"Barker\&Step"}$$

$$s_{TR}(t) = \begin{cases} \frac{A}{2}(s(t)+1)\ for\ 0 \le t \le T \\ 0\ \ for\ T < t \le T + T_h \end{cases} \qquad s_{TR}(t) = \begin{cases} \frac{A}{2}(s(t)+1)\ for\ 0 \le t < T \\ A/2\ for\ T < t < T + T_h \end{cases} \tag{7}$$

$$\text{Fitting function "1"} \qquad \text{Fitting function "2"}$$

$$y_{SQ}(t) = \begin{cases} a_1 t + a_2 t^{0.9} + a_3 t^{0.8}\ for\ 0 \le t \le T \\ y_{SQ}(T) - a_1 t - a_2 t^{0.9} - a_3 t^{0.8}\ \ for\ T < t \le T + T_h \end{cases} \qquad y_{SQ}(t) = a_1 t + a_2 t^{0.9} + a_3 t^{0.8}\ \forall t$$

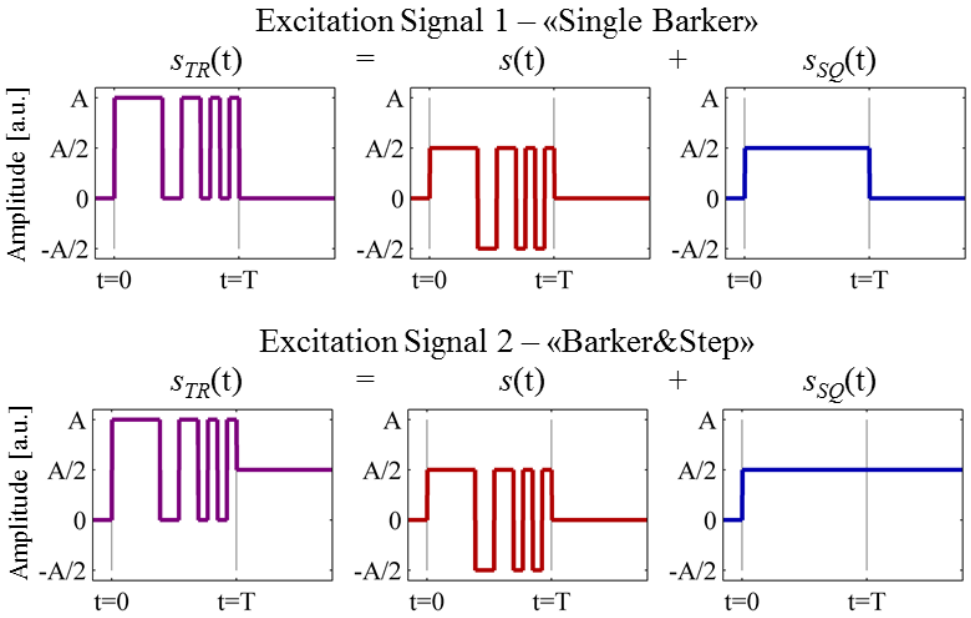

Fig. 3 Decomposition of the true excitation signal $s_{TR}(t)$ into a proper coded excitation $s(t)$ plus a square pulse $s_{SQ}(t)$ for the two procedures proposed: "Single Barker" and "Barker&Step"

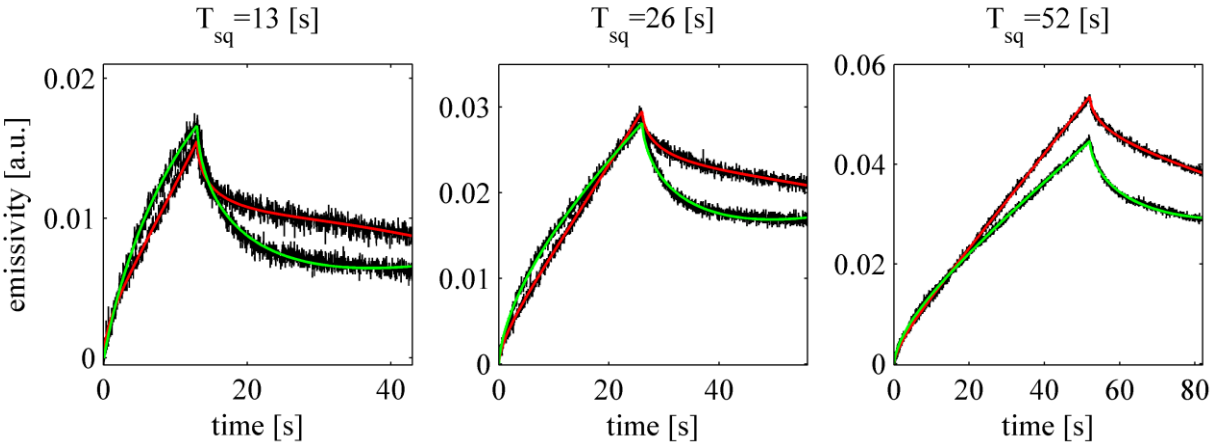

Fig. 4. Examples of the application of the fitting function 1 (see Eq.7) to various step-heating data. Green fitting curves correspond to a pixel over a defect, red fitting curves correspond to a pixel on a sound area.

The powers used in the fitting functions has been previously optimized using Step-Heating data acquired on the same sample. Results of this analysis with the fitting function "1" are reported in Fig.4 for various Step durations; the fitting function follows both the rise and decay parts of the curves very well. Since the best fitting function could depend on both the sample and the heating source power, the preliminary optimization of the powers should be done for each set-up.

The results of the applications of the fitting functions to PuCT data collected by using the excitation signals "Single Barker" and "Barker&Step" are reported in Fig.5. After the fitting procedure, the separate contributions from the coded excitation and that of the square excitation are differentiated. This is discussed further in Section IV in terms of SNR and quality of impulse response reconstruction.

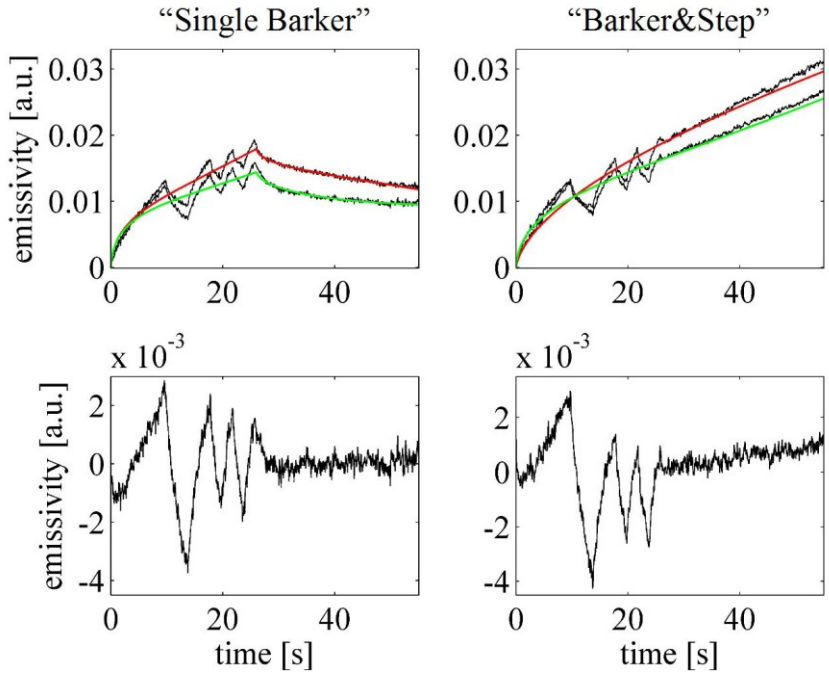

Fig. 5. (top) Application of the fitting procedures to typical single-pixel curves obtained with the "Single Barker" and the "Barker&Step" excitations: green fitting curves correspond to a pixel over a defect, red fitting curves correspond to a pixel on a defect-free area. (bottom) Resulting coded output signals $y(t)$ after the removal of the respective square pulse outputs $y_{SQ}(t)$ for the pixel over a defect.

III.B Sidelobes minimization using a Wiener Filter

It is important to reduce the noise level in the sidelobes in order to obtain the best estimation of the impulse response. To tackle this problem, one strategy is to use Wiener Filtering approach [44–46]. Fig.6 shows the $\widetilde{\delta}(t)$ obtained using either a standard matched filter (black) and a Wiener Filter (red). While the main lobe is unaltered by the Wiener filter, a sidelobe suppression level of over 30dB is obtained. From a mathematical point of view, the use of the Wiener filter simply consists of replacing the matched filter $\Psi(t)$ with a new one, $\Psi_W(t)$, having the same phase profile in the frequency domain but a different spectrum amplitude. For the results reported in the next Section, we used a Wiener filter $\Psi_W(t)$ defined in the frequency domain as follows:

$$\Psi_W(f) = \frac{\Psi(f)}{|\Psi(f)|^2 + a + b \cdot \mathrm{f}}, \tag{8}$$

where a and b are two regularization parameters that damp the oscillations in the $\tilde{\delta}(t)$; b penalizing high-frequency oscillations.

To summarize, by combining the square pulse response removal, the correct pulse-compression procedure and the Wiener filter, the gain provided by the use of coded excitation is optimized both in terms of SNR and impulse response quality.

Figure 7 qualitatively illustrates the effect of the overall pulse compression procedure on defect detection and resolution by reporting a graphical comparison between thermograms collected during the application of the Barker code excitation and after pulse compression. The experimental set-up described in the next section was used to collect data and many expected features are immediately evident in the compressed thermograms: (1) the "compression" of the thermal response of each pixel in the time dimension; (2) the higher SNR/contrast of both the defects and the single pixel time-trends; (3) the resulting improved spatial resolution.

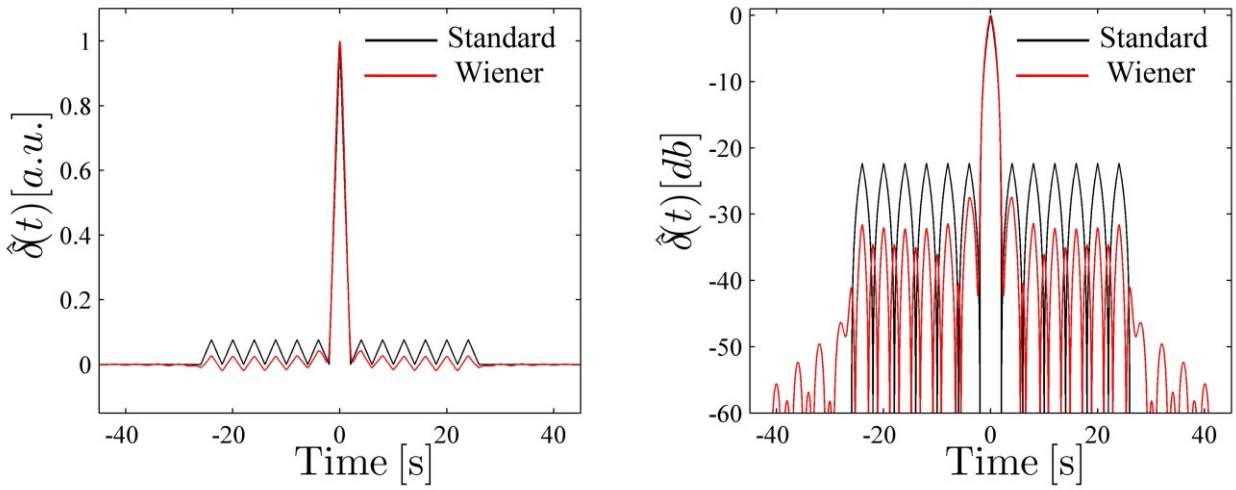

Fig.6: Comparison between simulated $\tilde{\delta}(t)$ obtained by using the Standard matched filter approach (black) and Wiener filter (red). The plot on the left is in linear scale, the plot on the right is in logarithmic scale.

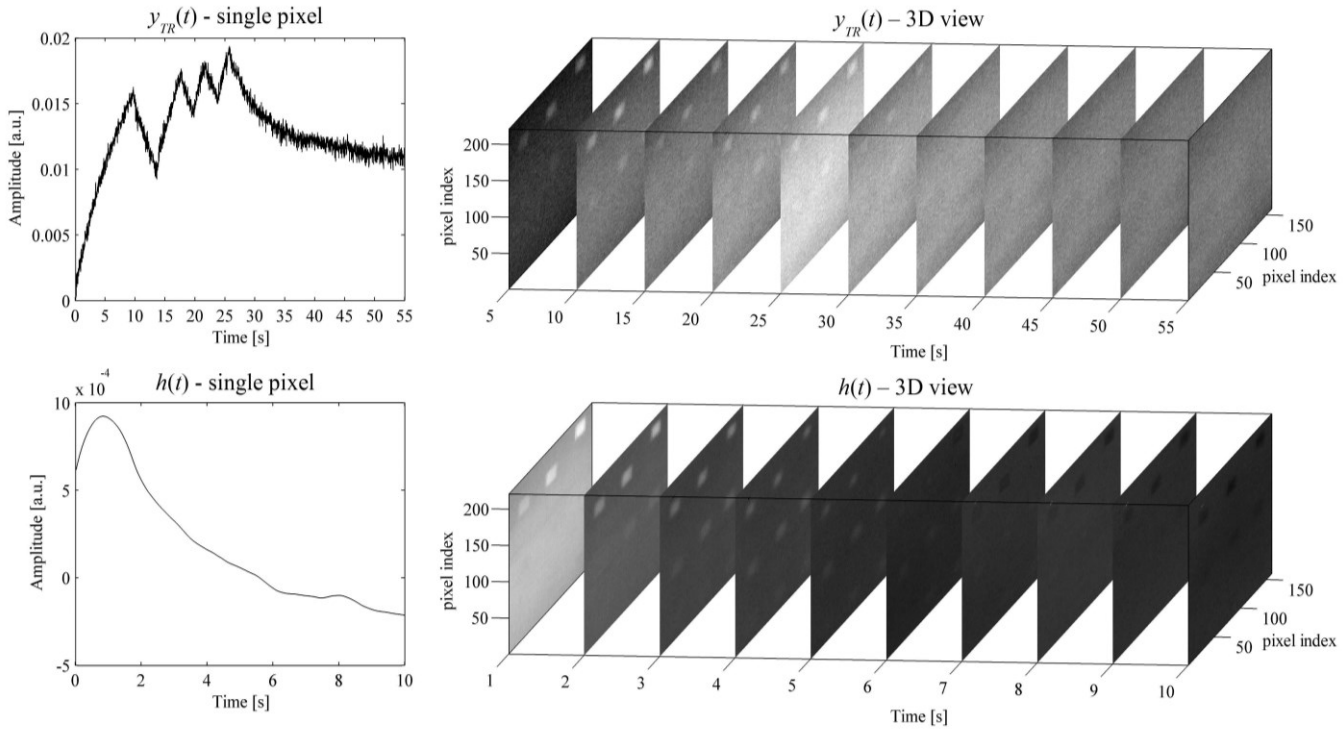

Fig.7. Comparison between thermograms collected at different times during the application of the Barker code excitation (top) and thermograms retrieved after pulse compression (bottom).

IV RESULTS

IV.A Experimental set-up

A sketch of the experimental set-up used is shown in Fig.8. The signal generation/acquisition was managed by means of a National Instrument PCI-6711 Arbitrary Waveform Generation (AWG) board and by a NI-1433 Camera Link Frame Grubber, both connected to a central PC and managed through a custom Labview virtual instrument. The coded excitation was input into a power amplifier consisting on a TDK Lambda GEN 750W power supply that fed four 50 W LED chips placed at ~30 cm from the SUT. The AWG board provided also a clock signal for a Xenics Onca-MWIR-InSb IR camera that acquired the thermograms.

The carbon fiber composite laminate sample contained twelve plies of carbon fiber fabric with an areal density of 0200 g/m^2. Its lateral dimensions were 240mm×200mm and the thickness was ~2.80mm. The fibers orientations were 0° and 90° and the matrix was an Epoxy Resin RIM 935.The laminate was made by vacuum assisted resin infusion and it was cured at room temperature and postured at 110°C for two hours, in order to obtain a fully cured system. The artificial delaminations were realized by inserting square pieces of Teflon tape with lateral dimensions of 20mm×20mm and thickness equal to 75 μm between the plies. Nine artificial defects were inserted at increasing depths: the outer was placed under the 2nd ply at a depth $d \sim 0.46\ mm$, the inner under the 10th ply at a depth $d \sim 2.3\ mm$ see Figure 9.

The thermal diffusivity α of the SUT was estimated by applying an empirical law obtained for a CFRP sample at time $t_{0.5}$:

$$\alpha = \left(2.829 * 10^{-9}\right) * Vf + 1.247 * 10^{-7} \left[\frac{m^2}{s}\right] \tag{9}$$

where V_f is the fiber volume fraction (in our case $V_f \sim 0.5$) [47].

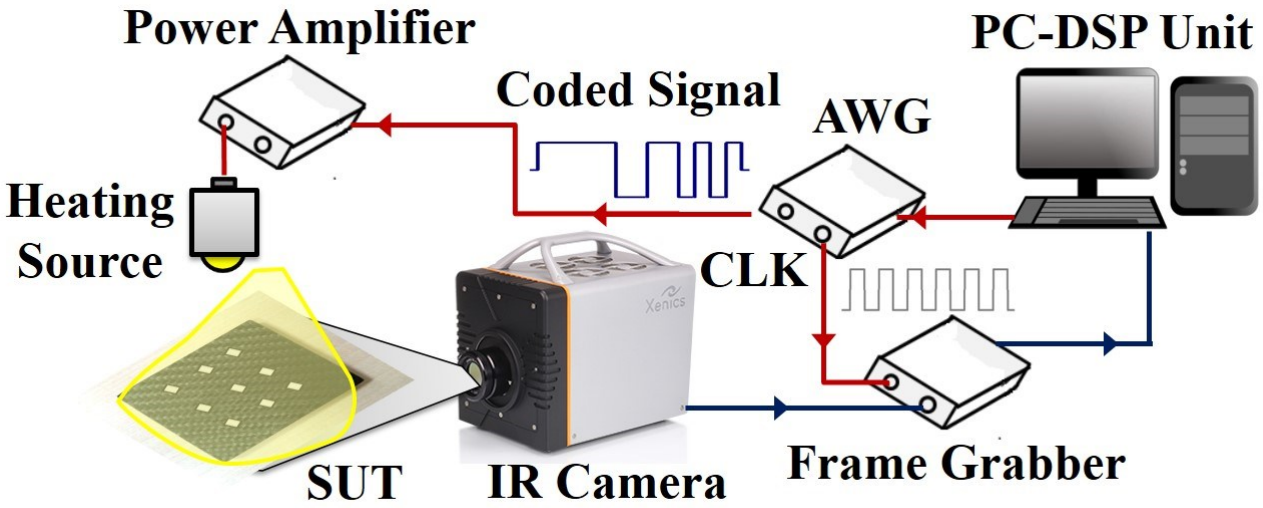

Fig.8: Sketch of the experimental setup. The heating source consisting of 4 50 W LED chips placed at ~30 cm from the SUT and the IR camera are synchronously driven by the signals provided by an AWG board. The data generation and acquisition was controlled using Labview™ Software.

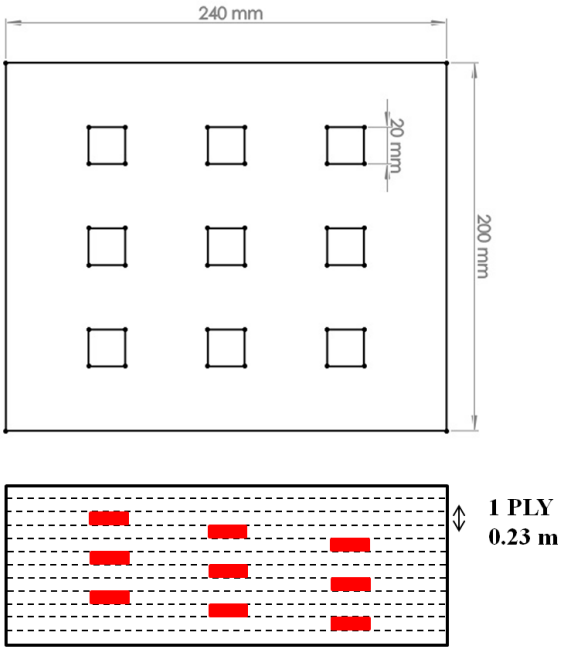

Fig.9: Detailed sketch of the SUT.

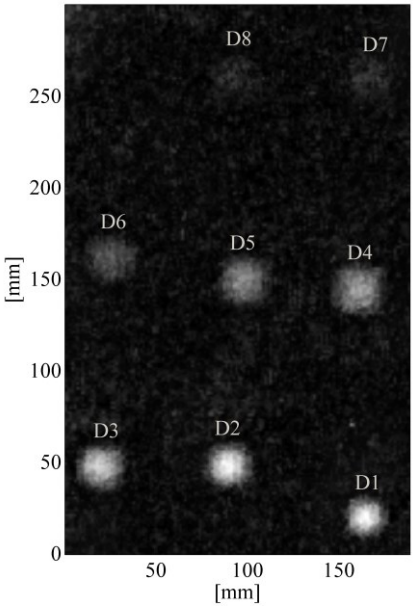

Fig.10: Example of the thermal image of the sample from the Barker&Step sequence at the instant of maximum SNR value for the D7 defect. The defects were labeled from D1 to D9 depending on the increasing depth from the inspection surface.

IV.B Comparison between the various pulse-compression procedures

In this Subsection, we report a comparison between the results achieved by applying the procedures "Single Barker" and "Barker&Step" introduced in the previous Sections and by following the conventional "State-of-the-art" procedure, i.e. the one with the truncated acquisition and the linear fitting for DC removal. This comparison aims to identify which technique assures the highest SNR and the best estimation of the pixels'

impulse response. To fulfil this objective, we firstly located the position of each defect within the sample and then analyzed their corresponding impulse responses. Figure 10 shows a thermal image of the sample obtained after pulse compression. All the defects were visible and they were sorted according to their relative depth from the inspection side: D1 is the outer defect, and D9 is the inner one. For each defect, an area of 3x3 pixels was associated and an averaged impulse response was calculated following the three procedures ("State-of-the-art", "Single Barker", "Barker&Step").

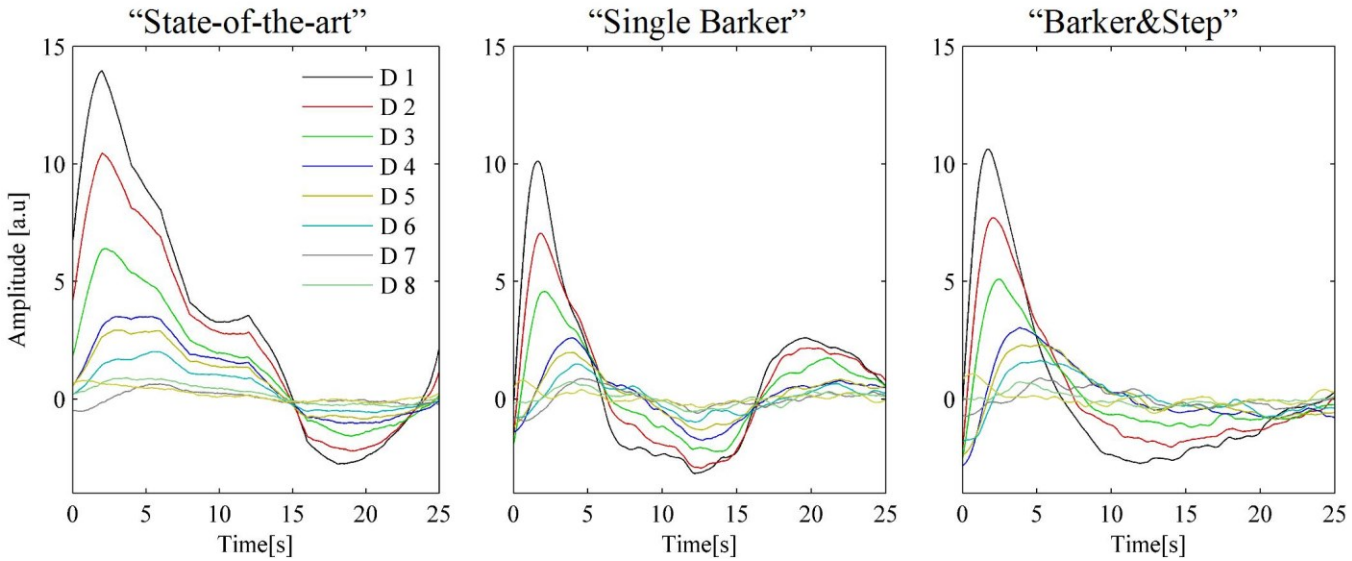

Fig.11: Defects impulse responses obtained by exploiting (left) the "State-of-the-art" procedure, (middle) the "Single Barker", (right) the "Barker&Step", for defects at increasing depth (D1 to D8).

The resulting impulse responses for the defects D1-D8 are reported in Figure 11. Please note that Defect 9 was not considered for the comparison purpose. This is because its SNR was very low. The combined application of (1) the polynomial fitting, (2) the full pulse-compression procedure and (3) the Wiener filter makes the impulse responses achieved with the "Single Barker" and "Barker&Step" procedures more regular than those retrieved with the "State-of-the-art". In particular, while all the "State-of-the-art" curves exhibited abrupt variations and tended to have a quite similar time-behavior irrespective of the defect depth, the impulse responses attained by means of the "Barker&Step" are quite similar to those typically find in PT experiments, see fig.16, and the dependence of the signal shape from the defect depth is evident, as expected due to the diffusion time and the dispersive nature of the thermal phenomenon (see Subsection II.A). Larger oscillations were instead still present in the "Single Barker" results. We concluded therefore that the polynomial fitting applied to the "Barker Step" procedure optimizes removal of the square pulse response $y_{SQ}(t)$ among the three methods. Hence the mathematical noise associated to a non-perfect separation of the coded excitation response $y(t)$ is minimized.

To quantitatively corroborate this result, the same analysis was repeated in terms of SNR, defined as follows:

$$SNR_{D_k} = \frac{h_{D_k}(t) - \bar{h}(t)}{\sigma_h(t)} \tag{10}$$

where $h_{D_k}(t)$ is the impulse response of the k-th defect averaged over the 3x3 pixel region, $\bar{h}(t)$ is the impulse response averaged over all the SUT area and $\sigma_h(t)$ is its standard deviation. The resulting SNR curves for the D1-D8 defects are shown in Figure 12.

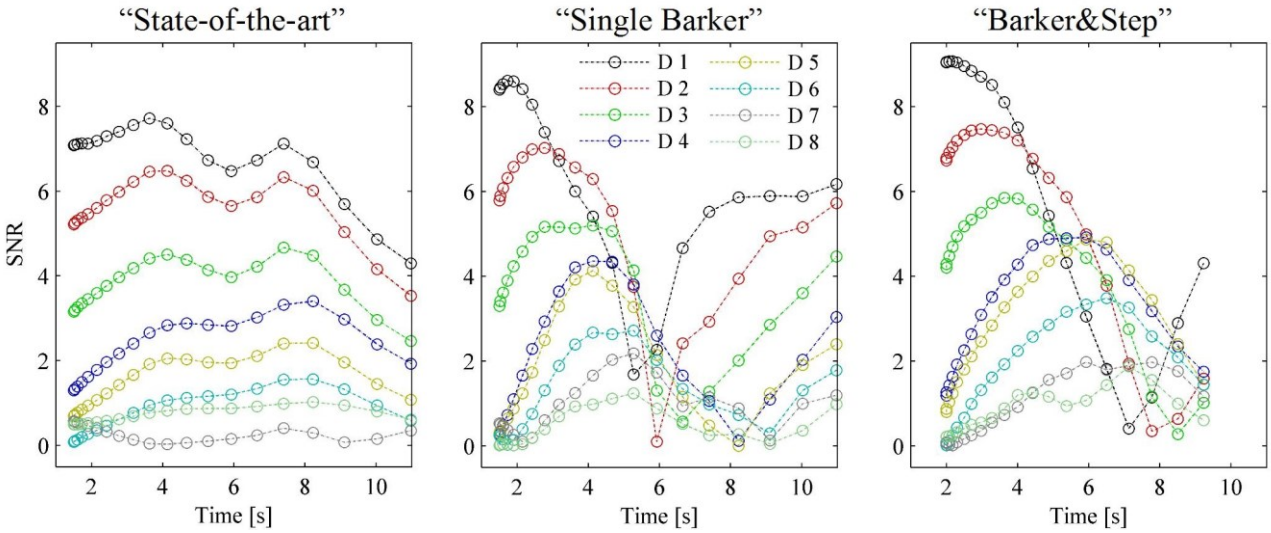

Fig.12: Defects SNR time-curves obtained by exploiting (left) the "State-of-the-art" procedure, (middle) the "Single Barker", (right) the "Barker&Step" for defects at increasing depth (D1 to D8).

This analysis confirmed that the "Barker&Step" procedure achieved the best results among the three techniques analyzed: the "State-of-the-art" curves exhibited the lowest SNRs, especially for inner defects. Increasingly there was not a clear dependence of the maximum of the SNR on the defect depth d, which ideally should follow a relation like that indicated in Eq. 6 for the parameter $t_{max}(d)$. Conversely, the "Single Barker" and the "Barker&Step" procedures showed an enhanced defect discrimination capability in terms of both SNR and time of the maximum SNR, even at the cost of the increasing of measurement time (in this case for 25 seconds) in order to collect the decay of the coded excitation response. This last aspect is better illustrated in Figure 13 where the values of $t_{max}(d)$ estimated from the SNR curves for the "State-of-the-art" and the "Barker&Step" techniques are reported. While in the former case $t_{max}(d)$ weakly depends on the defects depth assuming only two values for the eight defects considered, for the "Barker&Step" procedure an evident correlation between $t_{max}(d)$ and d is found, see Fig.13-a. It can be seen also that for the outer defects (D1-D4), $t_{max}(d)$ fits well with the quadratic law reported in Eq.6. In particular, by analyzing only these four defects an "effective" thermal diffusivity $\alpha_{fit} = 0.088\ [mm^2/s]$ is retrieved, close to the expected one $\alpha_{th} = 0.125\ [mm^2/s]$.

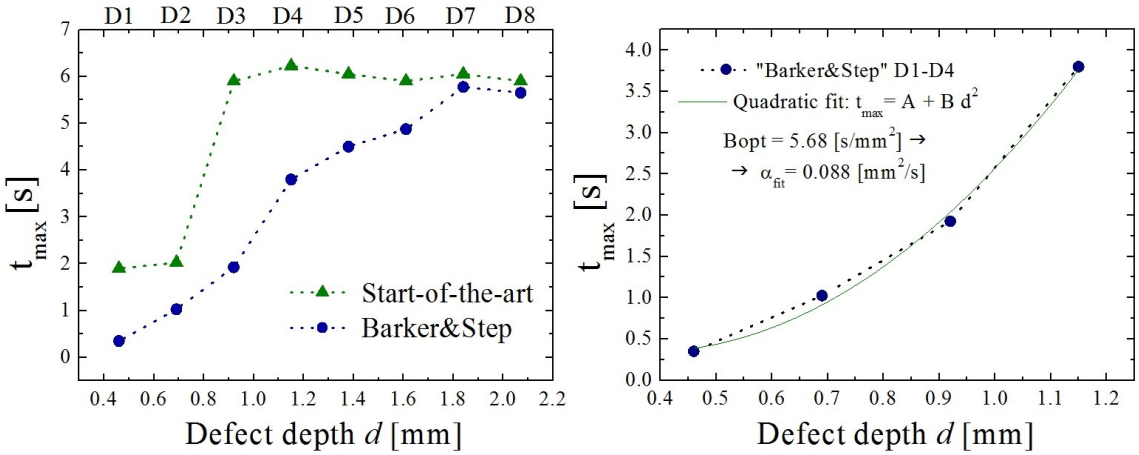

Fig.13: Values of time of the maximum SNR $t_{max}(d)$ estimated from the SNR curves for the "State-of-the-art" and the "Barker&Step" techniques are reported. the "Barker&Step" technique showed an enhanced defect discrimination capability in terms of time of the maximum SNR (Left). For the outer defects (D1-D4), the $t_{max}(d)$ trend fits well with the quadratic law reported in Eq.6 (Right) .

IV.C Comparison between pulse-compression and pulsed thermography

To corroborate the results reported in the previous section, a comparison between PuCT and PT has been executed. Conventional PT data were collected on the same composite sample by using a pair of high-energy flash lamps with a total energy of 6 $[kJ]$ (Hensel EH Pro 6000 flash system), placed at ~ 40 $[cm]$ from the sample surface. Thermograms were acquired at 100 Hz for 25 seconds by means of a FLIR SC7000 camera, equipped with a 3-5µm InSb sensor with a resolution of 512x640 pixels. Some basic image processing was applied (time and 2D spatial smooth to remove high frequency noise components). This system was chosen to obtain a similar total heating energy for both PT and PuCT "Barker&Step" cases. While PT provides 6 kJ, the PuCT energy consists in this case of the sum of two terms: the energy of the modulated Barker excitation plus the energy of the square pulse. The peak power during coded excitation is equal to 200 W and the power of the square pulse is fixed to 100 W. By using a 13-bit Barker code ($B[n] = \{1,1,1,1,1,0,0,1,1,0,1,0,1\}$) with a single bit duration $T_{bit} = 2$ $[s]$, the resulting coded excitation lasts 26 $[s]$ with a total energy equal to 3.6 $[kJ]$. By assuming $T_h = 25$ $[s]$, the energy of the step is 2.5 $[kJ]$, for a total energy of 6.1 $[kJ]$. So, although a precise comparison is not possible since the two light sources and the respective set-ups are different, the heating energy is roughly equal for the PT and the PuCT "Barker&Step" method. Note also that in the "Single Barker" case the heating energy is only 3.6 $[kJ]$, and it should be also considered that the square response is removed leading to a minor effective coded energy and to a further information to be processed. Nevertheless, an accurate comparison between PT and PuCT in terms of heating energy lies beyond the scope of this article. The goal here is to verify how close are the results of the proposed PuCT procedure to that of the PT technique.

Analogously to Fig. 10, Fig. 14 shows the thermogram obtained with PT at the instant of maximum SNR value for the D7 defect. In Fig.15 the defects' impulse responses and the corresponding SNR time curves measured with the PT set-up are reported and compared with those retrieved by applying PuC to the Barker&Step data, see Figs. 11,12. The PT and the PuCT results are in very good agreement both in terms of image quality and SNR.

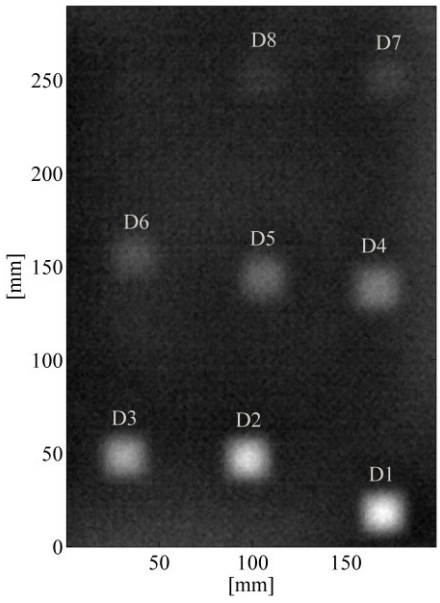

Fig.14: Example of the thermal image (512x640 pixels) of the SUT from the 6 kJ Pulsed Thermography sequence at the instant of maximum SNR value for the D7 defect. The defects were labeled from D1 to D9 depending on the increasing depth from the inspection surface.

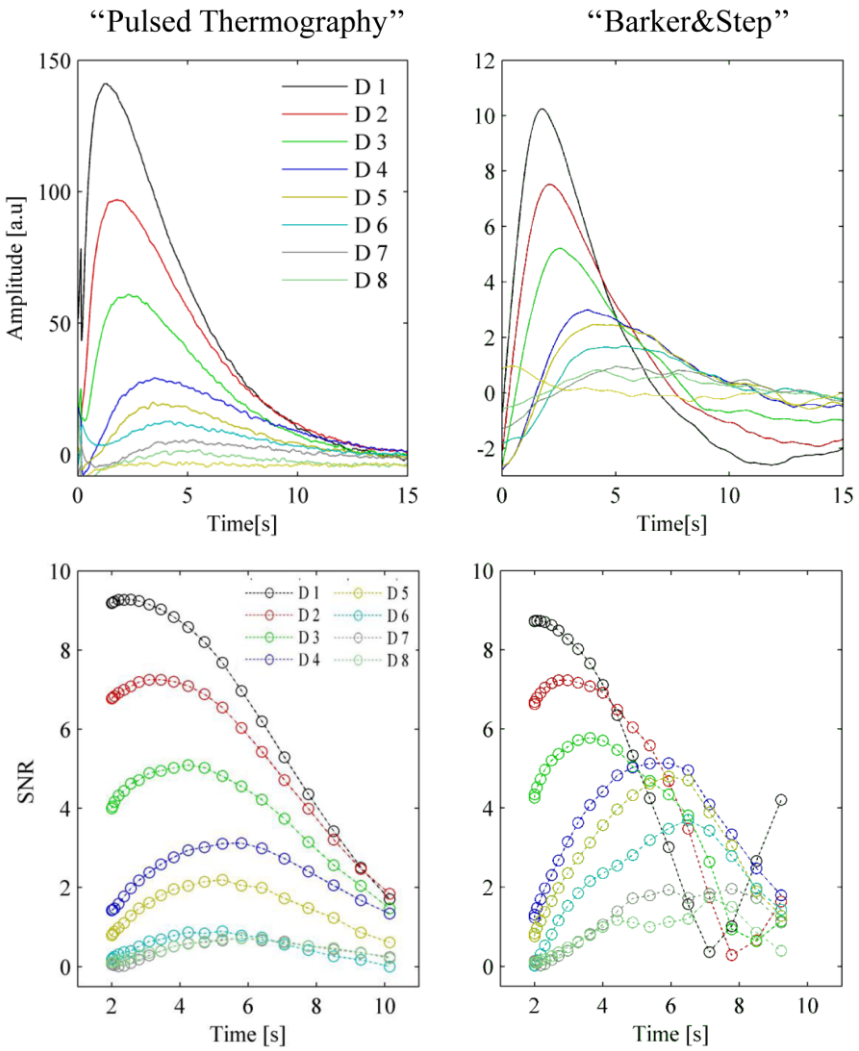

Fig.15: Comparison of conventional (left) 6kJ pulsed thermography and PuCT (right) exploiting the "Barker&Step" procedure. Top: Defects impulse responses for defects at increasing depth (D1 to D8). Bottom: Defects SNR time-curves obtained for the same defects.

In the PuCT time trends some effect of the PuC sidelobes is seen, but at the same time the SNR is higher than for the PT case for deep defects. Of the three PuCT approaches considered, the "Barker & Step" results are the most similar to those of PT.

CONCLUSIONS

In this paper the application of the pulse compression technique to active thermographic NDE is analyzed both theoretically and experimentally and three different measurement procedures are compared. Some strategies capable of improving the performance of the pulse-compression active thermography with respect to the state-of-the-art techniques are introduced and the experimental results reported demonstrate the gain provided by such procedures. The optimization of the fitting function for the selection of the correct coded excitation output, together with the application of both a suitable pulse compression algorithm and of a Wiener filter for sidelobe suppression, allows the thermal impulse response of the sample under inspection to be reconstructed with an improved SNR and enhanced fidelity. Hence, both the defect detection and the defect characterization tasks exhibit better performance than with the standard procedure. The optimized pulse-compression procedure is also compared with pulsed thermography, showing a good agreement between the

results obtained with the two different approaches. In perspective, pulse compression thermography can be further improved by using coded excitations with an arbitrary power spectrum to increase the SNR of the deepest defects [35,48] and by reducing even more the sidelobes.

ACKNOWLEDGMENTS

The authors acknowledge partial financial support from Fondazione Carit. The authors thank dr. Matthias Goldhammer for contributing actively to the pulsed thermography measurements and for the scientific .

REFERENCES

[1] X.P. V Maldague, Introduction to NDT by active infrared thermography, Mater. Eval. 60 (2002) 1060–1073.
[2] X. Maldague, Applications of Infrared Thermography, Trends Opt. Nondestruct. Test. (2000) 591–609.
[3] C. Meola, G.M. Carlomagno, Recent advances in the use of infrared thermography, Meas. Sci. Technol. 15 (2004) R27–R58.
[4] X. Maldague, S. Marinetti, Pulse phase infrared thermography, J. Appl. Phys. 79 (1996) 2694. doi:10.1063/1.362662.
[5] Y. He, M. Pan, F. Luo, Defect characterisation based on heat diffusion using induction thermography testing, Rev. Sci. Instrum. 83 (2012).
[6] I. Zainal Abidin, G. Yun Tian, J. Wilson, S. Yang, D. Almond, Quantitative evaluation of angular defects by pulsed eddy current thermography, NDT E Int. 43 (2010) 537–546.
[7] D. Bates, G. Smith, D. Lu, J. Hewitt, Rapid thermal non-destructive testing of aircraft components, Compos. Part B Eng. 31 (2000) 175–185.
[8] J.A. Schroeder, T. Ahmed, B. Chaudhry, S. Shepard, Non-destructive testing of structural composites and adhesively bonded composite joints: pulsed thermography, Compos. Part A Appl. Sci. Manuf. 33 (2002) 1511–1517.
[9] N.P. Avdelidis, B.C. Hawtin, D.P. Almond, Transient thermography in the assessment of defects of aircraft composites, NDT E Int. 36 (2003) 433–439.
[10] M. Genest, M. Martinez, N. Mrad, G. Renaud, A. Fahr, Pulsed thermography for non-destructive evaluation and damage growth monitoring of bonded repairs, Compos. Struct. 88 (2009) 112–120.
[11] R. Usamentiaga, P. Venegas, J. Guerediaga, L. Vega, I. Lo, Feature extraction and analysis for automatic characterization of impact damage in carbon fiber composites using active thermography, NDT E Int. 54 (2013) 123–132.
[12] S.M. Shepard, <title>Advances in pulsed thermography</title>, in: A.E. Rozlosnik, R.B. Dinwiddie (Eds.), International Society for Optics and Photonics, 2001: pp. 511–515.
[13] X. Maldague, F. Galmiche, A. Ziadi, Advances in pulsed phase thermography, Infrared Phys. Technol. 43 (2002) 175–181.
[14] N.P. Avdelidis, D.P. Almond, A. Dobbinson, B.C. Hawtin, Pulsed thermography : philosophy , qualitative quantitative analysis on aircraft materials & applications, 2006.
[15] D.L. Balageas, Defense and illustration of time-resolved pulsed thermography for NDE, QIRT J. 6733 (2012) 1–1.
[16] D. Wu, G. Busse, Lock-in thermography for nondestructive evaluation of materials, Rev. Générale Therm. 37 (1998) 693–703.
[17] T. Sakagami, S. Kubo, Applications of pulse heating thermography and lock-in thermography to quantitative nondestructive evaluations, Infrared Phys. Technol. 43 (2002) 211–218.
[18] C. Meola, G.M. Carlomagno, A. Squillace, A. Vitiello, Non-destructive evaluation of aerospace materials with lock-in thermography, Eng. Fail. Anal. 13 (2006) 380–388.
[19] S. Pickering, D. Almond, Matched excitation energy comparison of the pulse and lock-in thermography NDE techniques, NDT E Int. 41 (2008) 501–509.
[20] G. Pitarresi, Lock-In Signal Post-Processing Techniques in Infra-Red Thermography for Materials Structural Evaluation, Exp. Mech. 55 (2015) 667–680.
[21] N. Tabatabaei, A. Mandelis, Thermal-wave radar: A novel subsurface imaging modality with extended depth-resolution dynamic range, Rev. Sci. Instrum. 80 (2009) 1–11.
[22] N. Tabatabaei, A. Mandelis, Thermal coherence tomography using match filter binary phase coded diffusion waves, Phys. Rev. Lett. 107 (2011) 1–5.
[23] R. Mulaveesala, S. Tuli, Theory of frequency modulated thermal wave imaging for nondestructive subsurface defect detection, Appl. Phys. Lett. 89 (2006).
[24] V.S. Ghali, N. Jonnalagadda, R. Mulaveesala, Three-dimensional pulse compression for infrared nondestructive testing, IEEE Sens. J. 9 (2009) 832–833.
[25] V.S. Ghali, S.S.B. Panda, R. Mulaveesala, Barker coded thermal wave imaging for defect detection in carbon fibre-

reinforced plastics, Insight - Non-Destructive Test. Cond. Monit. 53 (2011) 621–624.
[26] D. Hutchins, P. Burrascano, L. Davis, S. Laureti, M. Ricci, Coded waveforms for optimised air-coupled ultrasonic nondestructive evaluation, Ultrasonics. 54 (2014) 1745–1759.
[27] R. Mulaveesala, S. Venkata Ghali, Coded excitation for infrared non-destructive testing of carbon fiber reinforced plastics, Rev. Sci. Instrum. 82 (2011).
[28] J. Gong, J. Liu, L. Qin, Y. Wang, Investigation of carbon fiber reinforced polymer (CFRP) sheet with subsurface defects inspection using thermal-wave radar imaging (TWRI) based on the multi-transform technique, NDT E Int. 62 (2014) 130–136.
[29] J.A. Siddiqui, V. Arora, R. Mulaveesala, A. Muniyappa, Infrared Thermal Wave Imaging for Nondestructive Testing of Fibre Reinforced Polymers, Exp. Mech. 55 (2015) 1239–1245.
[30] R. Yang, Y. He, Pulsed Inductive Thermal Wave Radar (PI-TWR) Using Cross Correlation Matched Filtering in Eddy Current Thermography, Infrared Phys. Technol. 71 (2015) 469–474.
[31] K. Chatterjee, S. Tuli, S.G. Pickering, D.P. Almond, A comparison of the pulsed, lock-in and frequency modulated thermography nondestructive evaluation techniques, NDT E Int. 44 (2011) 655–667.
[32] R.H. Barker, Group synchronizing of binary digital systems, Commun. Theory. (1953) 273–287.
[33] R. Turyn, J. Storer, On binary sequences, Proc. Am. Math. Soc. 19 (1960) 394–399.
[34] H.S. Carslaw, J.C. Jaeger, Conduction of heat in solids, Oxford Clarendon Press. 1959, 2nd Ed. (1959).
[35] P. Burgholzer, Thermodynamic Limits of Spatial Resolution in Active Thermography, Int. J. Thermophys. 36 (2015) 2328–2341.
[36] A. Salazar, Energy propagation of thermal waves, Eur. J. Phys. 27 (2006) 1349–1355.
[37] F. Lopez, V. De Paulo Nicolau, C. Ibarra-Castanedo, X. Maldague, Thermal-numerical model and computational simulation of pulsed thermography inspection of carbon fiber-reinforced composites, Int. J. Therm. Sci. 86 (2014) 325–340.
[38] S.M. Shepard, J.R. Lhota, B.A. Rubadeux, D. Wang, T. Ahmed, Reconstruction and enhancement of active thermographic image sequences, Opt. Eng. 42 (2003) 1337.
[39] D. Balageas, J.M. Roche, Q.I. Thermography, 2014-Common tools for quantitative time resolved pulse and step heating thermography part 1 theoretical basics, (2015).
[40] G.L. Turin, An Introduction to Matched Filters, IRE Trans. Inf. Theory. 6 (1960) 311–329.
[41] R.Y. Chiao, X. Hao, Coded Excitation for Diagnostic Ultrasound : A System Developer ' s Perspective Preprint for 2003 IEEE Ultrasonics Symposium Preprint for 2003 IEEE Ultrasonics Symposium, IEEE Trans. Ultrason. Ferroelectr. Freq. Control. 52 (2003) 160–170.
[42] T. Misaridis, J.A. Jensen, Use of modulated excitation signals in medical ultrasound. Part III: High frame rate imaging, IEEE Trans. Ultrason. Ferroelectr. Freq. Control. 52 (2005) 208–218.
[43] M. Ricci, L. Senni, P. Burrascano, Exploiting pseudorandom sequences to enhance noise immunity for air-coupled ultrasonic nondestructive testing, IEEE Trans. Instrum. Meas. 61 (2012) 2905–2915.
[44] B. Haider, P.A. Lewin, K.E. Thomenius, Pulse elongation and deconvolution filtering for medical ultrasonic imaging, IEEE Trans. Ultrason. Ferroelectr. Freq. Control. 45 (1998) 98–113.
[45] E. Sekko, G. Thomas, A. Boukrouche, A deconvolution technique using optimal Wiener filtering and regularization, Signal Processing. 72 (1999) 23–32.
[46] M.L. Oelze, Bandwidth and resolution enhancement through pulse compression, IEEE Trans. Ultrason. Ferroelectr. Freq. Control. 54 (2007) 768–781.
[47] G. Wróbel, Z. Rdzawski, Determination of thermal diffusivity of carbon/epoxy composites with different fiber content using transient thermography, J. Achiev. Mater. Manuf. Eng. 37 (2009) 518–525.
[48] M. Ricci, S. Callegari, S. Caporale, M. Monticelli, L. Battaglini, M. Eroli, L. Senni, R. Rovatti, G. Setti, P. Burrascano, Exploiting Non-Linear Chirp and sparse deconvolution to enhance the performance of pulse-compression ultrasonic NDT, IEEE Int. Ultrason. Symp. IUS. (2012) 1489–1492.